Roton-mediated soliton bound states in binary dipolar condensates

R. M. V. Röhrs and R. N. Bisset

Universität Innsbruck, Fakultät für Mathematik, Informatik und Physik, Institut für Experimentalphysik, 6020 Innsbruck, Austria

(Received 4 October 2025; accepted 18 February 2026; published 19 March 2026)

We investigate the formation of bound states between dark-antidark solitary waves in two-component dipolar Bose-Einstein condensates. The excitation spectrum contains density and spin branches and a rotonic feature of the spin branch enables long-range soliton interactions, giving rise to multiple bound states for a single pair, each with a distinct separation. We show that these bound states originate from periodic modulations of the intersoliton potential, while individual solitons are surrounded by spatial spin-density oscillations. Both features provide direct signatures of the spin roton. Collisions between unbound solitons probe this potential, with dipolar interactions enforcing universal bouncing at low velocities, independent of soliton sign, whereas nondipolar solitons may either transmit or bounce. This distinct behavior offers a realistic path to confirming spin rotons experimentally.

DOI: 10.1103/dddk-qym1

I. INTRODUCTION

Solitons are localized waveforms that maintain their shape during propagation and after collisions, arising from a balance between nonlinearity and dispersion. They appear in diverse physical systems, including water waves [1,2], conducting polymers [3,4], and nonlinear optics [5], and they play a fundamental role in nonlinear wave phenomena. Ultracold gases provide an especially versatile platform for studying solitons, offering unparalleled control over experimental conditions [6,7].

Bose-Einstein condensates (BECs) with dipole-dipole interactions promise fundamentally novel possibilities for the study of solitons. Condensates made of strongly dipolar atoms, namely chromium [8,9], dysprosium [10,11], or erbium [12] are nowadays available in numerous laboratories. Even in dilute regimes, the long-ranged and anisotropic interactions give rise to fascinating phenomena—perhaps more familiar in condensed-matter settings—including a roton-maxon dispersion relation [13–18], liquidlike droplets [11,19–22], and supersolidity [23–25]. When the dispersion relation has a rotonic character, static density oscillations are anticipated to form surrounding a soliton core and predictions have been made for two dark solitons to form a bound state [26,27].

A parallel research thrust in multicomponent BECs is the study of vector solitons, excitations that span multiple components through intercomponent coupling. In two-component (binary) mixtures, the excitation spectrum splits into a density branch, corresponding to in-phase density fluctuations, and a spin branch, corresponding to out-of-phase fluctuations. The spin branch, characterized by fluctuations of the spin density $n_1 - n_2$, plays a central role in both the internal structure of vector solitons and their interactions. An important experimentally realized example in binary condensates is the dark-antidark soliton [28–34], a solitary wave in which one miscible component exhibits a phase step and density dip, while the other shows a corresponding density peak. Of particular interest are bound states of oppositely polarized dark-antidark soliton pairs (also termed dark-dark solitons) [35–37], which have been observed experimentally in counterflowing BECs [28,29]. These bound states result from attractive intersoliton interactions and give rise to dynamics and stability properties distinct from conventional single-component solitons [38]. Setting the stage for the present work, we emphasize that, although both binary condensates and single-component dipolar condensates can host solitary wave bound states, the underlying physical mechanisms differ. Moreover, dipolar mixtures have recently been cooled to quantum degeneracy [39–47] and their capacity to realize vector solitons remains unexplored.

We theoretically investigate dark-antidark solitary waves and their bound states in two-component dipolar BECs confined to quasi-one-dimensional geometries. We compare the density profiles of isolated solitons in nondipolar and dipolar systems. In the nondipolar case, the soliton width diverges as the spin branch softens, whereas dipolar interactions generate spin rotons that suppress this broadening and instead induce spatial spin-density oscillations extending far from the core. We derive the dispersion relations of the uniform system and calculate the interaction potential between two solitons, showing that a spin roton is associated with periodic modulations of the interaction potential, which enable the formation of at least three distinct bound states. Finally, we study soliton collisions, revealing qualitatively new behavior arising from dipolar interactions.

II. FORMALISM

A. System and interactions

We study a distinguishable mixture of two BECs in an infinite-tube geometry at the mean-field level. Each

Published by the American Physical Society under the terms of the Creative Commons Attribution 4.0 International license. Further distribution of this work must maintain attribution to the author(s) and the published article's title, journal citation, and DOI.

component is labeled by $i \in \{1, 2\}$ and atoms in component i at position $\mathbf{x}$ are subject to interactions from atoms in component j at position $\mathbf{x}'$ according to

$$\Phi_{ij}^{3D}(\mathbf{x}) = g_{ij}|\Psi_j(\mathbf{x})|^2 + \int d\mathbf{x}'\, U_{ij}^{3D}(\mathbf{x}-\mathbf{x}')|\Psi_j(\mathbf{x}')|^2, \quad (1)$$

where $\Psi_j(\mathbf{x})$ is the wave function of component j and $g_{ij} = 4\pi a_{ij}\hbar^2/m$ is the contact coupling constant determined by the s-wave scattering lengths a_{ij}. The dipolar interactions are described by

$$U_{ij}^{3D}(\mathbf{r}) = \frac{3g_{ij}^{dd}}{4\pi}\frac{1-3\cos^2\vartheta}{r^3}, \quad (2)$$

with $g_{ij}^{dd} = 4\pi a_{ij}^{dd}\hbar^2/m$, where $a_{ij}^{dd} = \mu_0\mu_i\mu_j m/12\pi\hbar^2$ are the dipole lengths associated with magnetic moments μ_i. For simplicity, we assume both components have the same mass m. The quantity ϑ represents the angle between the dipole alignment direction $\hat{z}$ and the vector $\mathbf{r} = \mathbf{x} - \mathbf{x}'$, representing the relative position of the interacting particles.

B. Quasi-one-dimensional GPEs

The quasi-one-dimensional geometry is realized by a cylindrically symmetric harmonic trap with transverse confinement frequencies $\omega_y = \omega_z \equiv \omega$ and an unconfined axial direction $\omega_x = 0$. In this setting, each condensate wave function separates into a radial and an axial part, the former given by harmonic-oscillator ground states with transverse oscillator length $l = \sqrt{\hbar/m\omega}$ and the latter by $\psi_i(x)$. After integrating out the transverse degrees of freedom and neglecting the radial zero-point energy, the system reduces to coupled one-dimensional Gross-Pitaevskii equations (GPEs)

$$i\hbar\partial_t\psi_i = \left(-\frac{\hbar^2}{2m}\partial_x^2 + \sum_j \frac{g_{ij}n_j}{2\pi l^2} + \sum_j \Phi_{ij}\right)\psi_i, \quad (3)$$

where $n_j(x) = |\psi_j(x)|^2$ is the one-dimensional (1D) density and $N_j = \int dx\, n_j(x)$ is the particle number of component j. The effective 1D dipolar potential $\Phi_{ij}(x)$ is obtained via a convolution involving the Fourier transformation $\mathcal{F}$ and its inverse $\mathcal{F}^{-1}$ (see [48–50] for the one-component case):

$$\Phi_{ij}(x) = \mathcal{F}^{-1}\{U_{ij}(k)\mathcal{F}[|\psi_j|^2]\},$$
$$U_{ij}(k) = \frac{g_{ij}^{dd}A_\alpha}{2\pi l^2}[1 + 3Q^2\exp Q^2\mathrm{Ei}(-Q^2)], \quad (4)$$

with $A_\alpha = [1-3\cos^2\alpha]/2$, $Q = \frac{1}{2}k^2l^2$, and $\mathrm{Ei}(x) = -\int_{-x}^{\infty} dt\, e^{-t}/t$. The angle α specifies the orientation of the dipoles relative to the tube axis $\hat{x}$; here we focus on the case of dipoles aligned perpendicular to the axis, i.e., $\alpha = \pi/2$.

C. Numerics and parameters

The coupled one-dimensional Gross-Pitaevskii equations (3) are solved using a fourth-order Runge-Kutta method on a uniform spatial grid with periodic boundary conditions. Following Refs. [26,27,38], at-rest solitons are prepared by imprinting a π-phase step in the appropriate component at each time step during imaginary-time evolution.

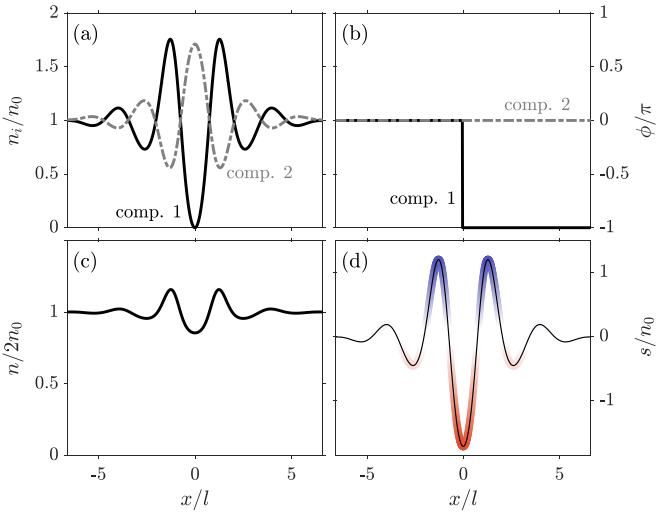


FIG. 1. Isolated dark-antidark soliton in a binary dipolar condensate. (a) Density profiles: component 1 (solid) and component 2 (dot-dashed). (b) Wave function phase profiles. (c) Total-density profile. (d) Spin-density profile. Colors match the spin densities shown in Figs. 3(i)–3(iii) and 5(b). Scattering lengths: $\{a_{11}, a_{12}, a_{22}\}/a_0 = \{140, 105, 140\}$.

To isolate the effects of dipole-dipole interactions, we use the same trapping frequencies and average densities in all simulations (although in Appendix A we consider other densities). Specifically, we consider balanced populations $N_1 = N_2 \equiv N/2$, with average per-component density $n_0 = N/2L = 667$ atoms $\mu\mathrm{m}^{-1}$ and a single transverse trapping frequency $\omega = 2\pi \times 500\,\mathrm{Hz}$. In the dipolar case, a roton in the spin branch of the dispersion relation can occur over a broad range of parameters but emerges more readily when the components have imbalanced dipole moments [51–53]. As a representative example, we study a binary dipolar condensate based on ^{162}Dy, with $\mu_1 = 9.93\,\mu_B$, $\mu_2 = 0$, and $m = 162u$, where u is the atomic mass unit. This situation could be experimentally realized using spin mixtures [54]. However, our results should be qualitatively applicable across a wide range of dipolar- and nondipolar-dipolar mixtures [39–47], provided a spin roton is present. To demonstrate this generality, we investigate two additional parameter regimes in Appendix A. For the nondipolar binary condensate, we set $\mu_1 = \mu_2 = 0$ and take ^{87}Rb ($m = 87u$) as our reference system.

III. RESULTS

A. Isolated dark-antidark solitons

In single-component dipolar BECs, spatial density oscillations arise near boundaries and defects such as hard walls [55], quantum vortices [56,57], and soliton cores [26,27]. These features are associated with roton modes in the dispersion relation [57,58], analogous to the connection between rotons and spatial density oscillations in superfluid helium [59,60]. Similarly, Fig. 1 shows that, in a binary dipolar condensate, a dark-antidark soliton is a localized spin-density perturbation that generates spatial spin-density oscillations around its core, analogous to the density oscillations predicted around a half-quantum vortex [61].

Figure 1 displays the (a) density and (b) phase distributions of a dark-antidark soliton at rest. The dipolar component (component 1) hosts a dark soliton with a π phase step, while the nondipolar component (component 2) forms an antidark structure with uniform phase. Figure 1(c) shows that, while this excitation generates small modulations in the total density $n(x) = n_1(x) + n_2(x)$, Fig. 1(d) reveals pronounced oscillations of the spin density $s(x) = n_1(x) - n_2(x)$. Since the sign of the spin density also oscillates, we define the soliton sign as the sign of $s(x)$ at its core, determined by which components carry the phase jump. For the present example, at the core $s(x) < 0$, which we define as a *negative-core* dark-antidark soliton. Conversely, when the soliton core exhibits $s(x) > 0$, we refer to it as a *positive-core* dark-antidark soliton. The characteristic spacing between the resulting peaks and troughs of $s(x)$ can be understood in terms of the system's dispersion relations.

B. Derivation of dispersion relations

Binary condensates exhibit two gapless Goldstone dispersion relations, arising from the two spontaneously broken gauge symmetries associated with each order parameter. Because of the intercomponent coupling, one branch is predominantly associated with fluctuations of the total density $n(x)$, while the other corresponds to fluctuations of the spin density $s(x)$. Using Bogoliubov theory, we derive an expression for the density (+) and spin (−) dispersion relation branches (see Appendix B):

$$\epsilon_{\pm}^2(k) = \frac{\epsilon_1^2 + \epsilon_2^2}{2} \pm \frac{1}{2}\sqrt{\left(\epsilon_1^2 - \epsilon_2^2\right)^2 + 4G_{12}G_{12}\frac{\hbar^4 k^4}{m^2}}, \quad (5)$$

where

$$\epsilon_i^2(k) = \frac{\hbar^2 k^2}{2m}\left(\frac{\hbar^2 k^2}{2m} + 2G_{ii}(k)\right), \quad (6)$$

with

$$G_{ij}(k) = \sqrt{n_i n_j}\left(\frac{g_{ij}}{2\pi l^2} + U_{ij}(k)\right). \quad (7)$$

C. Role of dispersion relations in soliton structure

Here we compare the role of the dispersion relations in determining the structure of dark-antidark solitons in dipolar mixtures and contrast this with that of nondipolar mixtures. Figure 2 shows the dispersion relations [Eq. (5)] and the corresponding spin density of isolated solitons for (a) nondipolar and (b) dipolar mixtures for several values of a_{12}. In both cases, the spin branches ϵ_- (solid lines, shaded from dark to light with increasing a_{12}) soften as the miscible-immiscible threshold is approached ($a_{12}^c = \sqrt{a_{11}a_{22}} = 100a_0$ for the nondipolar case and $a_{12}^c \approx 110a_0$ for the dipolar case).

For nondipolar mixtures [Fig. 2(a1)], the spin branch smoothly approaches the free-particle dispersion (thin dashed line), with the spin healing length $\xi_s = \hbar/\sqrt{2mn_0\delta g/\pi l^2}$ diverging at the transition where $\delta g \equiv (\sqrt{g_{11}g_{22}} - g_{12}) = 0$. In contrast, the dipolar mixture [Fig. 2(b1)] develops a spin-roton minimum [51–53,62], which deepens with increasing a_{12} and bends the branch below the free-particle (noninteracting) curve, corresponding to effectively repulsive interactions

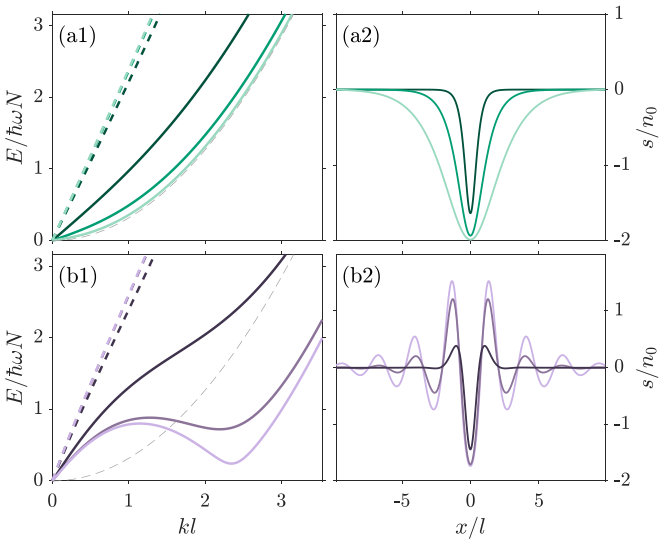


FIG. 2. Relationship between the dispersion relations (left) and spin density (right) for a soliton in a binary condensate, shown without (a) and with (b) dipolar interactions. (a1) Dispersion relations for nondipolar mixtures with $a_{12} = [70, 95, 99]\,a_0$ from dark to light and fixed intraspecies interactions $a_{11} = a_{22} = 100\,a_0$. Solid (dashed) lines denote spin (density) branches; thin dashed line shows free-particle reference. (a2) Corresponding spin density profiles of dark-antidark solitons. (b1) Dispersion relations for binary dipolar condensate with $a_{12} = [70, 105, 108.4]\,a_0$, from dark to light, with $a_{11} = a_{22} = 140\,a_0$. (b2) Corresponding spin-density profiles of dark-antidark solitons.

at small k but attractive interactions at large k. This can be understood by noting from Eqs. (5)–(7) that deviations from the free particle energy, $\epsilon_0 = \hbar^2 k^2/2m$, arise from $G_{ij}(k)$ and the changing sign of $\epsilon_-(k) - \epsilon_0(k)$ is caused by the momentum dependence of the dipole-dipole interactions $U_{ij}(k)$ [63]. In both systems, the density branches ϵ_+ (dashed lines) depend only weakly on a_{12}.

The corresponding spin-density soliton profiles reflect these contrasting dispersion relations [64]. In the nondipolar case [Fig. 2(a2)], the soliton width grows with increasing ξ_s, while the central spin density approaches $s = -2n_0$, consistent with a magnetic soliton of nearly constant total density [65]. In dipolar mixtures [Fig. 2(b2)], the roton generates spin-density oscillations of wavelength $\lambda_{\rm rot}/l \approx 2.7$ around the soliton core. The width of the central minimum remains $\sim\lambda_{\rm rot}$, but the decay length of the modulations increases with increasing roton depth. Note that, at the miscible-immiscible threshold, spin-density fluctuations cost zero energy, signaling a transition to the alternating-domain supersolid phase [62,66,67]. The presence of spin rotons not only shapes individual solitons but also plays a crucial role in mediating the interactions between two solitons, setting the stage for the formation of multiple bound states.

D. Multiple bound states and soliton-pair interactions

The upper panels of Fig. 3 illustrate representative examples of three types of excited bound states with distinct equilibrium separations. Panel (i) shows solitons oscillating through one another at $a_{12}/a_0 = 95$, analogous to magnetic

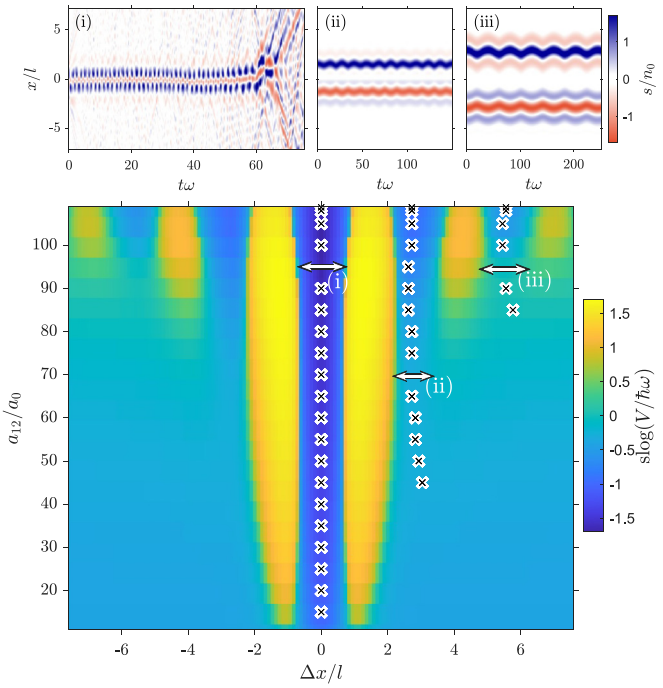


FIG. 3. (Main panel) Intersoliton potential versus separation and interspecies scattering length for binary dipolar condensate. Crosses mark local minima where stationary-state bound states exist. Panels (i)–(iii) show oscillations of two solitons about the first, second, and third minima, respectively, for selected a_{12} values (see double-headed arrows), with spin-density color coding as in Fig. 1(d). The spin density is shown as a function of position and time. Intraspecies scattering lengths are fixed at $a_{11} = a_{22} = 140a_0$.

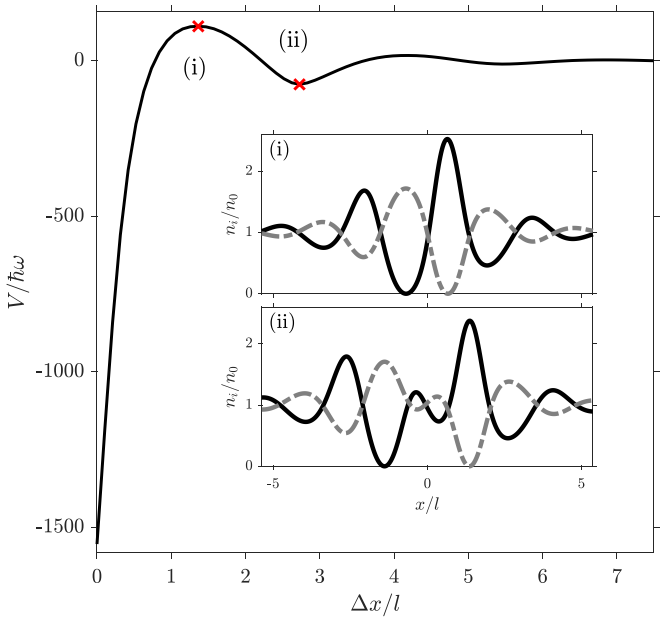


FIG. 4. Intersoliton potential versus soliton separation for a binary dipolar condensate. Three minima are present, corresponding to three regions where bound states can form. The insets show the density of component 1 (solid) and component 2 (dashed) of soliton pairs with separations $\Delta x/l \approx 1.35$ and $\Delta x/l \approx 2.7$, corresponding to a maximum (i) and a minimum (ii) in V, respectively. Contact interaction parameters: $\{a_{11}, a_{12}, a_{22}\}/a_0 = \{140, 105, 140\}$.

soliton bound states in binary nondipolar condensates [38]. Panels (ii) and (iii) depict long-range bound states oscillating about equilibrium positions $\Delta x/l \approx 2.7$ and $\Delta x/l \approx 5.4$ for $a_{12}/a_0 = 70$ and $a_{12}/a_0 = 95$, respectively, where $\Delta x = x_2 - x_1$ with x_i the position of soliton i. Because dipolar interactions break integrability, these structures are not true solitons in the strict sense and radiate energy through phonon emission [26]. Such phonons can be seen as fluctuations in the spin density far from the solitons in Fig. 3(i), even for early times. Dissipation-driven acceleration eventually pushes oscillating solitons beyond their escape velocity [26,68], as seen in Fig. 3(i) at $t\omega \approx 60$. This counterintuitive behavior indicates that dark-antidark solitons in binary dipolar BECs have negative effective masses, similar to dark solitons in single-component dipolar BECs [26,27] and dark-antidark soltions in binary BECs [65]. We confirm this numerically for our system in Appendix C.

The three different types of bound states with distinct separations can be understood by considering the effective intersoliton potential

$$V(\Delta x, a_{12}) = \mathrm{sgn}(m_{\mathrm{sol}})\, E(\Delta x, a_{12}), \tag{8}$$

which is calculated from the GPEs with

$$E(\Delta x, a_{12}) = E_{\mathrm{tot}}(\Delta x, a_{12}) - E_{\mathrm{sep}}(a_{12}), \tag{9}$$

where E_{tot} is the system energy of two zero-velocity solitons separated by a distance Δx and E_{sep} is the system energy of two well-separated solitons, ensuring $E = 0$ at maximal separation. For dark-antidark solitons, the effective mass satisfies $m_{\mathrm{sol}} < 0$ and its sign is included in Eq. (8) to render the direction of the restoring force for bound-state oscillations in Fig. 3 more transparent.

The main panel in Fig. 3 presents $V(\Delta x, a_{12})$ for two opposite-sign solitons across a broad range of intercomponent scattering lengths a_{12}, plotted using a symmetric logarithmic transform,

$$\mathrm{slog}(x) = \mathrm{sgn}(x) \log_{10}(\sqrt{x^2 + 1}), \tag{10}$$

to highlight small-magnitude features.

The modulation prominence of $V(\Delta x)$—related to the depth of the spin roton—increases up to the roton-instability threshold $a_{12}^{\mathrm{c}} \approx 110\, a_0$ [69]. A minimum at $\Delta x = 0$ exists for all a_{12}. As a_{12} increases, additional local minima emerge: one at $|\Delta x|/l \approx 2.7$ for $a_{12} \gtrsim 45\, a_0$ and another at $|\Delta x|/l \approx 5.4$ for $a_{12} \gtrsim 85\, a_0$, resulting in three distinct potential valleys (crosses). These valleys indicate the distinct separations at which soliton bound states form.

E. Origin of multiple bound states

To elucidate the origin of multiple minima in the intersoliton potential $V(\Delta x)$, we examine the case $a_{12}/a_0 = 105$ in Fig. 4, where minima occur at $|\Delta x|/l \approx [0, 2.7, 5.4]$. In the presence of spin rotons, a single soliton induces a spatially oscillating spin-density profile (recall Figs. 1 and 2) that acts as a polarized background. If a second soliton is placed at a location where this background aligns with its polarization distribution, only minor adjustments of the spin texture are

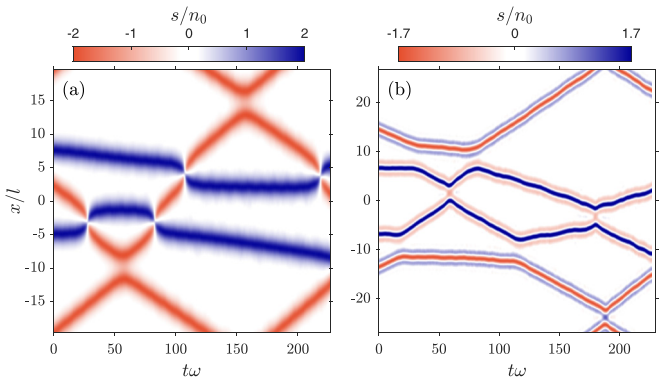


FIG. 5. Unbound collisional dynamics involving two initially nonmoving positive-core (blue) and two initially moving negative-core (red) dark-antidark solitons, shown (a) without and (b) with dipolar interactions. Spin density is shown as a function of position and time. Contact interaction parameters: (a) $\{a_{11}, a_{12}, a_{22}\}/a_0 = \{100, 95, 100\}$; (b) $\{a_{11}, a_{12}, a_{22}\}/a_0 = \{140, 95, 140\}$.

required [see Fig. 4(i)], lowering the energy cost compared to a homogeneous background (yielding $E < 0$, i.e., $V > 0$). Conversely, if the background is antialigned, large spin-density rearrangements are needed, raising the energy cost ($E > 0$, i.e., $V < 0$). In this case, the configuration shown in Fig. 4(ii) stabilizes a bound stationary state at $\Delta x/l \approx 2.7$, matching the roton wavelength $\lambda_{\rm rot}/l \approx 2.7$. Although this may seem counterintuitive, the restoring force is directed towards maxima of E (minima of V) due to the soliton's negative effective mass [see Eq. (8)].

When approaching the roton instability, $a_{12}^{\rm c}/a_0 \approx 110$, the decay length of the spatial spin density oscillations around the soliton core grows and so too does the number of alternating peaks and troughs of the intersoliton potential energy. For soliton pairs with like sign, minima in $V(\Delta x)$ develop at $|\Delta x| \approx (I + 1/2)\lambda_{\rm rot}$, whereas for opposite-sign pairs they occur at $|\Delta x| \approx I\lambda_{\rm rot}$, for $I = 0, 1, 2, \ldots$. Correspondingly, maxima in $V(\Delta x)$ occur at $|\Delta x| \approx I\lambda_{\rm rot}$ for like-sign solitons and at $|\Delta x| \approx (I + 1/2)\lambda_{\rm rot}$ for opposite-sign solitons.

Since spin rotons are predicted across a broad range of dipolar mixtures [62], our arguments imply that multiple bound states are expected not only in dipolar-nondipolar mixtures but also more generally. Additional simulations in Appendix A corroborate this, showing such bound states for $\mu_1/\mu_2 = -1$ and $\mu_1/\mu_2 \approx 0.2$.

F. Soliton collisions

True solitons can, in principle, emerge unscathed from collisions. However, the presence of dipolar interactions breaks integrability, so perfectly elastic collisions are not expected. Nevertheless, dark-antidark solitons may still survive collisions and thus serve as a probe of the intersoliton potential.

Figure 5 shows four dark-antidark solitons in each panel—two slowly moving negative-core solitons and two stationary positive-core solitons—in (a) the nondipolar reference system and (b) a binary dipolar condensate. In the nondipolar case, like-sign solitons bounce off each other, whereas opposite-sign solitons pass through (as predicted in Ref. [38]). With dipolar interactions present, however, they always bounce, independent of relative sign. The bouncing arises from the periodic maxima in the intersoliton potential V, which act as effective barriers. Crucially, universal low-velocity bouncing occurs because these maxima exist regardless of the soliton signs (see Sec. III E). For like-sign solitons, these maxima occur at integer multiples of $\lambda_{\rm rot}$; for opposite-sign solitons, they occur at half-integer multiples (see Fig. 4). Consequently, for the collisions shown in Fig. 5(b), the minimum separation before bouncing differs: $\Delta x \gtrsim \lambda_{\rm rot}$ for like-sign collisions and $\Delta x \gtrsim 1.5\lambda_{\rm rot}$ for opposite-sign collisions, suggesting that in both cases the second maxima are relevant at these velocities. These distinct collisional properties—especially when contrasted with the nondipolar case—could provide direct experimental evidence of the spin roton.

IV. CONCLUSION

We investigated the formation of multiple dark-antidark soliton bound states in two-component dipolar BECs. Using Bogoliubov theory, we derived the dispersion relation and linked the emergence of spin rotons to strong spatial spin-density oscillations around the soliton cores and modulations of the effective intersoliton potential, leading to the multiple bound states at distinct separations. Soliton collisions revealed that maxima in the intersoliton potential act as effective barriers, causing solitons to bounce regardless of relative sign. This behavior stands in sharp contrast to the nondipolar case—where opposite-sign solitons always pass through one another—thus providing a realistic pathway to probe and validate spin rotons in experiments.

Our results remain robust across a broad range of parameters, including densities well below those presented here. Moving toward higher densities, approaching the 3D-cigar regime, could test the persistence and stability of soliton bound states and may uncover new links between roton physics and nonlinear excitations.

ACKNOWLEDGMENTS

The authors acknowledge T. Billam, T. Bland, F. Ferlaino, L. B. Giacomelli, A. Madhusudan, N. Masalaeva, N. Parker, E. Poli, C. Qu, and P. Senarath Yapa for insightful discussions. This research was funded in whole or in part by the Austrian Science Fund (FWF) [10.55776/P36850].

DATA AVAILABILITY

The data that support the findings of this article are not publicly available upon publication because it is not technically feasible and/or the cost of preparing, depositing, and hosting the data would be prohibitive within the terms of this research project. The data are available from the authors upon reasonable request.

APPENDIX A: ADDITIONAL DIPOLAR MIXTURES

To demonstrate the generality of our findings to the case where both $\mu_1, \mu_2 \neq 0$, we consider two additional dipolar configurations. In the first, we choose $\{\mu_1, \mu_2\} = \{9.93, -9.93\}\mu_{\rm B}$ and an average per-component density $n_0 = 133$ atoms $\mu{\rm m}^{-1}$. Unless otherwise specified in the cap-

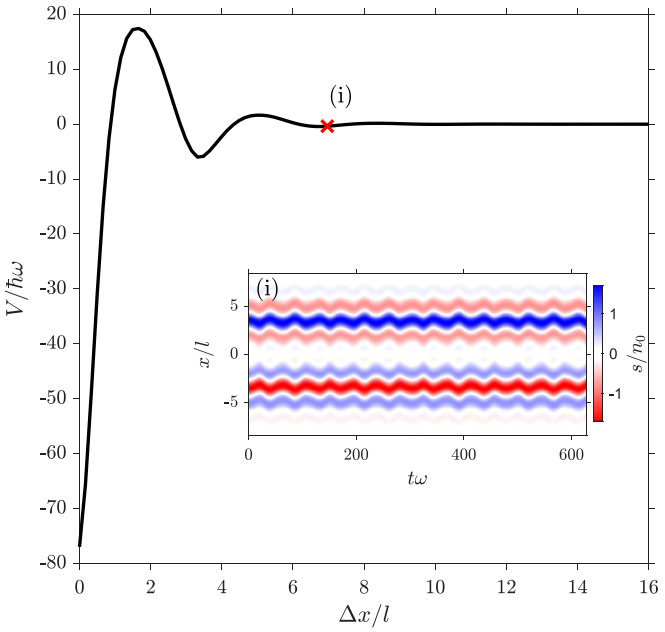


FIG. 6. Intersoliton potential versus soliton separation for a binary dipolar condensate with $\mu_1 = -\mu_2$. Four minima are present ($x_1 = 0,\ x_2 \approx 3.3,\ x_3 \approx 6.7,$ and $x_4 \approx 10.1$), corresponding to four regions where bound states can form. The inset shows example dynamics of the third bound state in an excited configuration, with the initial state position indicated as a cross in the main figure. Contact interaction parameters: $\{a_{11}, a_{12}, a_{22}\}/a_0 = \{140, 35, 140\}$.

tions, the remaining parameters are the same as in Sec. II C. Figure 6 shows the intersoliton potential between opposite-sign solitons, with four minima present, each representing a different bound state. Figure 6(i) shows an example of one such bound state in an excited configuration, oscillating about the third minimum in Fig. 6. Importantly, both the intersoliton potential and bound state behavior are qualitatively similar to the results presented in Fig. 3, despite the vastly different combination of dipole-dipole interaction parameters.

In the second configuration, we set $\{\mu_1, \mu_2\} = \{9.93, 2\}\mu_B$. Figure 7 shows an example of a bound state that remains stable until $t\omega \approx 70$. While these results may at first seem to suggest that a smaller difference between dipole

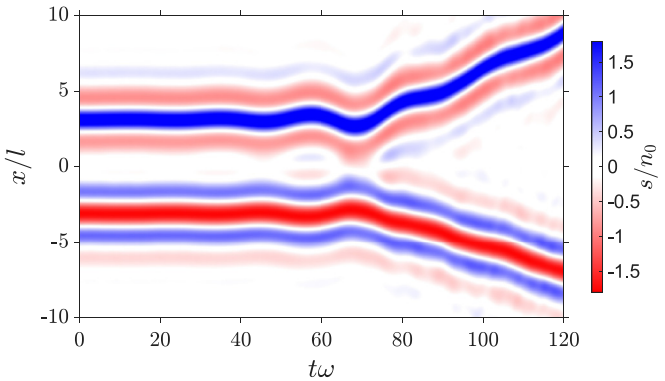


FIG. 7. Example of a bound state for $\{\mu_1, \mu_2\} = \{9.93, 2\}\mu_B$. This particular state becomes unbound at $t\omega \approx 70$. Contact interaction parameters: $\{a_{11}, a_{12}, a_{22}\}/a_0 = \{140, 121, 140\}$.

moments may lead to shorter bound-state lifetimes, we also sometimes observed relatively short-lived bound states for dipolar-nondipolar mixtures; hence further investigations are required to properly characterize lifetimes.

APPENDIX B: BOGOLIUBOV THEORY

This derivation of the dispersion relations for elementary excitations is similar to the one in Ref. [53] for antidipolar mixtures.

We look for solutions of Eq. (3) of the form

$$\psi_i(x,t) = (\sqrt{n_i} + \lambda[u_i(x)e^{-i\epsilon t/\hbar} - v_i^*(x)e^{i\epsilon^* t/\hbar}])e^{-i\mu_i t/\hbar}, \tag{B1}$$

where the condensate is perturbed via a small parameter λ around the average density n_i and u_i and v_i are the Bogoliubov amplitudes describing the perturbation. Inserting Eq. (B1) into Eq. (3) and keeping only terms up to linear order in λ, we can find the coupled equations by collecting terms evolving in time with $e^{-i\epsilon t/\hbar}$ and $e^{i\epsilon^* t/\hbar}$. Moving to momentum space $[\mathcal{F}_x[a(x)] = \tilde{a}(k)]$ we get

$$\epsilon\tilde{u}_i(k) = \frac{\hbar^2k^2}{2m}\tilde{u}_i(k) + \frac{\sqrt{n_i}}{2\pi l^2}\sum_j g_{ij}\sqrt{n_j}[\tilde{u}_j(k) - \tilde{v}_j(k)] + \sqrt{n_i}\sum_j U_{ij}(k)\sqrt{n_j}[\tilde{u}_j(k) - \tilde{v}_j(k)] \tag{B2}$$

and

$$\epsilon\tilde{v}_i(k) = -\frac{\hbar^2k^2}{2m}\tilde{v}_i(k) + \frac{\sqrt{n_i}}{2\pi l^2}\sum_j g_{ij}\sqrt{n_j}[\tilde{u}_j(k) - \tilde{v}_j(k)] + \sqrt{n_i}\sum_j U_{ij}(k)\sqrt{n_j}[\tilde{u}_j(k) - \tilde{v}_j(k)]. \tag{B3}$$

The coupled equations can be written as a matrix equation of the form $\epsilon\mathbf{w} = M\mathbf{w}$, where $\mathbf{w} = \{\tilde{u}_1, \tilde{u}_2, \tilde{v}_1, \tilde{v}_2\}$. The eigenvalues can be analytically calculated and the two

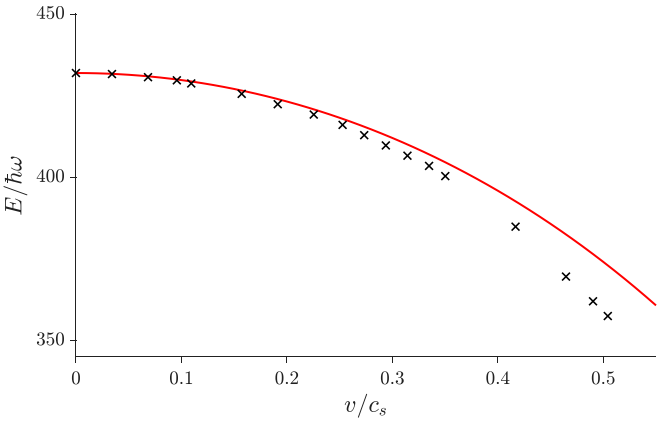


FIG. 8. Energy vs velocity for a dark-antidark soliton in a dipolar-nondipolar mixture. Black crosses show the numerical predictions, while the red solid line shows the analytic prediction for a magnetic soliton in a binary nondipolar BEC. Contact interaction parameters: $\{a_{11}, a_{12}, a_{22}\}/a_0 = \{140, 95, 140\}$.

positive-norm energy branches are then given by

$$\epsilon_{\pm}^2(k) = \frac{\epsilon_1^2 + \epsilon_2^2}{2} \pm \frac{1}{2}\sqrt{\left(\epsilon_1^2 - \epsilon_2^2\right)^2 + 4G_{12}G_{12}\frac{\hbar^4 k^4}{m^2}}, \quad \text{(B4)}$$

where the quasiparticle mode energies are

$$\epsilon_i^2(k) = \frac{\hbar^2 k^2}{2m}\left(\frac{\hbar^2 k^2}{2m} + 2G_{ii}(k)\right), \quad \text{(B5)}$$

with

$$G_{ij}(k) = \sqrt{n_i n_j}\left(\frac{g_{ij}}{2\pi l^2} + U_{ij}(k)\right). \quad \text{(B6)}$$

Equations (B4)–(B6) appear in the main text as Eqs. (5)–(7).

APPENDIX C: SOLITON EFFECTIVE MASS

Here, we investigate the sign of the effective mass of dark-antidark solitons in binary dipolar BECs. In Fig. 8, we numerically calculate the energy E (black crosses) of a single dark-antidark soliton as a function of its velocity v. For reference, we also plot the analytically predicted energy of a magnetic soliton in a binary nondipolar BEC (red line) [65]

$$E_{\rm ms}(v) = \alpha\sqrt{1 - v^2/c_{\rm s}^2}, \quad \text{(C1)}$$

where $c_{\rm s}$ is the spin speed of sound and we choose α such that $E_{\rm ms}(v = 0) = E(v = 0)$. We can see that $E(v)$ decreases as v increases, which indicates a negative effective mass according to the following expression [72]:

$$m_{\rm eff} = \frac{1}{v_{\rm s}}\frac{dE}{dv_{\rm s}}. \quad \text{(C2)}$$

[1] J. S. Russell, *The Wave of Translation in the Oceans of Water* (Trübner & Company, London, 1885).

[2] M. Ablowitz, *Nonlinear Dispersive Waves, Asymptotic Analysis and Solitons* (Cambridge University Press, Cambridge, UK, 2011).

[3] A. J. Heeger, S. Kivelson, J. R. Schrieffer, and W. P. Su, Solitons in conducting polymers, Rev. Mod. Phys. **60**, 781 (1988).

[4] T. Dauxois and M. Peyrard, *Physics of Solitons* (Cambridge University Press, Cambridge, UK, 2006).

[5] Y. S. Kivshar and G. P. Agrawal, *Optical Solitons: From Fibers to Photonic Crystal* (Academic Press, New York, 2003).

[6] L. Pitaevskii and S. Stringari, *Bose-Einstein Condensation and Superfluidity* (Oxford University Press, Oxford, 2016), Vol. 164.

[7] P. G. Kevrekidis, D. J. Frantzeskakis, and R. Carretero-González, *The Defocusing Nonlinear Schrödinger Equation: From Dark Solitons to Vortices and Vortex Rings* (SIAM, Philadelphia, PA, 2015).

[8] A. Griesmaier, J. Werner, S. Hensler, J. Stuhler, and T. Pfau, Bose-Einstein condensation of chromium, Phys. Rev. Lett. **94**, 160401 (2005).

[9] Q. Beaufils, R. Chicireanu, T. Zanon, B. Laburthe-Tolra, E. Maréchal, L. Vernac, J.-C. Keller, and O. Gorceix, All-optical production of chromium Bose-Einstein condensates, Phys. Rev. A **77**, 061601(R) (2008).

[10] M. Lu, N. Q. Burdick, S. H. Youn, and B. L. Lev, Strongly dipolar Bose-Einstein condensate of dysprosium, Phys. Rev. Lett. **107**, 190401 (2011).

[11] H. Kadau, M. Schmitt, M. Wenzel, C. Wink, T. Maier, I. Ferrier-Barbut, and T. Pfau, Observing the Rosensweig instability of a quantum ferrofluid, Nature (London) **530**, 194 (2016).

[12] K. Aikawa, A. Frisch, M. Mark, S. Baier, A. Rietzler, R. Grimm, and F. Ferlaino, Bose-Einstein condensation of Erbium, Phys. Rev. Lett. **108**, 210401 (2012).

[13] D. H. J. O'Dell, S. Giovanazzi, and G. Kurizki, Rotons in gaseous Bose-Einstein condensates irradiated by a laser, Phys. Rev. Lett. **90**, 110402 (2003).

[14] L. Santos, G. V. Shlyapnikov, and M. Lewenstein, Roton-Maxon spectrum and stability of trapped dipolar Bose-Einstein condensates, Phys. Rev. Lett. **90**, 250403 (2003).

[15] P. B. Blakie, D. Baillie, and R. N. Bisset, Roton spectroscopy in a harmonically trapped dipolar Bose-Einstein condensate, Phys. Rev. A **86**, 021604(R) (2012).

[16] L. Chomaz, R. M. van Bijnen, D. Petter, G. Faraoni, S. Baier, J. H. Becher, M. J. Mark, F. Waechtler, L. Santos, and F. Ferlaino, Observation of roton mode population in a dipolar quantum gas, Nat. Phys. **14**, 442 (2018).

[17] D. Petter, G. Natale, R. M. W. van Bijnen, A. Patscheider, M. J. Mark, L. Chomaz, and F. Ferlaino, Probing the roton excitation spectrum of a stable dipolar Bose gas, Phys. Rev. Lett. **122**, 183401 (2019).

[18] J.-N. Schmidt, J. Hertkorn, M. Guo, F. Böttcher, M. Schmidt, K. S. H. Ng, S. D. Graham, T. Langen, M. Zwierlein, and T. Pfau, Roton excitations in an oblate dipolar quantum gas, Phys. Rev. Lett. **126**, 193002 (2021).

[19] F. Wächtler and L. Santos, Quantum filaments in dipolar Bose-Einstein condensates, Phys. Rev. A **93**, 061603(R) (2016).

[20] R. N. Bisset, R. M. Wilson, D. Baillie, and P. B. Blakie, Ground-state phase diagram of a dipolar condensate with quantum fluctuations, Phys. Rev. A **94**, 033619 (2016).

[21] L. Chomaz, S. Baier, D. Petter, M. J. Mark, F. Wächtler, L. Santos, and F. Ferlaino, Quantum-fluctuation-driven crossover from a dilute Bose-Einstein condensate to a macrodroplet in a dipolar quantum fluid, Phys. Rev. X **6**, 041039 (2016).

[22] M. Schmitt, M. Wenzel, F. Böttcher, I. Ferrier-Barbut, and T. Pfau, Self-bound droplets of a dilute magnetic quantum liquid, Nature (London) **539**, 259 (2016).

[23] L. Tanzi, E. Lucioni, F. Famà, J. Catani, A. Fioretti, C. Gabbanini, R. N. Bisset, L. Santos, and G. Modugno, Observation of a dipolar quantum gas with metastable supersolid properties, Phys. Rev. Lett. **122**, 130405 (2019).

[24] F. Böttcher, J.-N. Schmidt, M. Wenzel, J. Hertkorn, M. Guo, T. Langen, and T. Pfau, Transient supersolid properties in an array of dipolar quantum droplets, Phys. Rev. X **9**, 011051 (2019).

[25] L. Chomaz, D. Petter, P. Ilzhöfer, G. Natale, A. Trautmann, C. Politi, G. Durastante, R. M. W. van Bijnen, A. Patscheider, M. Sohmen, M. J. Mark, and F. Ferlaino, Long-lived and transient supersolid behaviors in dipolar quantum gases, Phys. Rev. X **9**, 021012 (2019).

[26] K. Pawłowski and K. Rzążewski, Dipolar dark solitons, New J. Phys. **17**, 105006 (2015).

[27] T. Bland, M. J. Edmonds, N. P. Proukakis, A. M. Martin, D. H. J. O'Dell, and N. G. Parker, Controllable nonlocal interactions between dark solitons in dipolar condensates, Phys. Rev. A **92**, 063601 (2015).

[28] M. A. Hoefer, J. J. Chang, C. Hamner, and P. Engels, Dark-dark solitons and modulational instability in miscible two-component Bose-Einstein condensates, Phys. Rev. A **84**, 041605(R) (2011).

[29] D. Yan, J. Chang, C. Hamner, M. Hoefer, P. G. Kevrekidis, P. Engels, V. Achilleos, D. J. Frantzeskakis, and J. Cuevas, Beating dark–dark solitons in bose–einstein condensates, J. Phys. B: At. Mol. Opt. Phys. **45**, 115301 (2012).

[30] I. Danaila, M. A. Khamehchi, V. Gokhroo, P. Engels, and P. G. Kevrekidis, Vector dark-antidark solitary waves in multicomponent Bose-Einstein condensates, Phys. Rev. A **94**, 053617 (2016).

[31] A. Farolfi, D. Trypogeorgos, C. Mordini, G. Lamporesi, and G. Ferrari, Observation of magnetic solitons in two-component Bose-Einstein condensates, Phys. Rev. Lett. **125**, 030401 (2020).

[32] X. Chai, D. Lao, K. Fujimoto, R. Hamazaki, M. Ueda, and C. Raman, Magnetic solitons in a spin-1 Bose-Einstein condensate, Phys. Rev. Lett. **125**, 030402 (2020).

[33] G. C. Katsimiga, S. I. Mistakidis, T. M. Bersano, M. K. H. Ome, S. M. Mossman, K. Mukherjee, P. Schmelcher, P. Engels, and P. G. Kevrekidis, Observation and analysis of multiple dark-antidark solitons in two-component Bose-Einstein condensates, Phys. Rev. A **102**, 023301 (2020).

[34] S. M. Mossman, G. C. Katsimiga, S. I. Mistakidis, A. Romero-Ros, T. M. Bersano, P. Schmelcher, P. G. Kevrekidis, and P. Engels, Observation of dense collisional soliton complexes in a two-component Bose-Einstein condensate, Commun. Phys. **7**, 163 (2024).

[35] P. Öhberg and L. Santos, Dark solitons in a two-component Bose-Einstein condensate, Phys. Rev. Lett. **86**, 2918 (2001).

[36] E. G. Charalampidis, W. Wang, P. G. Kevrekidis, D. J. Frantzeskakis, and J. Cuevas-Maraver, SO(2)-induced breathing patterns in multicomponent Bose-Einstein condensates, Phys. Rev. A **93**, 063623 (2016).

[37] W. Wang, L.-C. Zhao, E. G. Charalampidis, and P. G. Kevrekidis, Dark–dark soliton breathing patterns in multicomponent bose–einstein condensates, J. Phys. B: At. Mol. Opt. Phys. **54**, 055301 (2021).

[38] R. M. V. Röhrs, C. Qu, and R. N. Bisset, Magnetic soliton molecules in binary condensates, Phys. Rev. A **112**, 053316 (2025).

[39] A. Trautmann, P. Ilzhöfer, G. Durastante, C. Politi, M. Sohmen, M. J. Mark, and F. Ferlaino, Dipolar quantum mixtures of erbium and dysprosium atoms, Phys. Rev. Lett. **121**, 213601 (2018).

[40] C. Ravensbergen, E. Soave, V. Corre, M. Kreyer, B. Huang, E. Kirilov, and R. Grimm, Resonantly interacting Fermi-Fermi mixture of ^{161}Dy and ^{40}K, Phys. Rev. Lett. **124**, 203402 (2020).

[41] T. Chalopin, T. Satoor, A. Evrard, V. Makhalov, J. Dalibard, R. Lopes, and S. Nascimbene, Probing chiral edge dynamics and bulk topology of a synthetic Hall system, Nat. Phys. **16**, 1017 (2020).

[42] G. Durastante, C. Politi, M. Sohmen, P. Ilzhöfer, M. J. Mark, M. A. Norcia, and F. Ferlaino, Feshbach resonances in an erbium-dysprosium dipolar mixture, Phys. Rev. A **102**, 033330 (2020).

[43] C. Politi, A. Trautmann, P. Ilzhöfer, G. Durastante, M. J. Mark, M. Modugno, and F. Ferlaino, Interspecies interactions in an ultracold dipolar mixture, Phys. Rev. A **105**, 023304 (2022).

[44] F. Schäfer, Y. Haruna, and Y. Takahashi, Realization of a quantum degenerate mixture of highly magnetic and nonmagnetic atoms, Phys. Rev. A **107**, L031306 (2023).

[45] M. Lecomte, A. Journeaux, J. Veschambre, J. Dalibard, and R. Lopes, Production and stabilization of a spin mixture of ultracold dipolar Bose gases, Phys. Rev. Lett. **134**, 013402 (2025).

[46] K. Xie, X. Li, Y.-Y. Zhou, J.-H. Luo, S. Wang, Y.-Z. Nie, H.-C. Shen, Y.-A. Chen, X.-C. Yao, and J.-W. Pan, Feshbach spectroscopy of ultracold mixtures of ^{6}Li and ^{164}Dy atoms, Phys. Rev. A **111**, 023327 (2025).

[47] J. Kalia, J. Rivera, R. R. Emran, W. J. S. Hernandez, K. Kwon, and R. J. Fletcher, Creation of a degenerate bose-bose mixture of erbium and lithium atoms, Phys. Rev. A **113**, 013321 (2026).

[48] S. Giovanazzi and D. H. O'Dell, Instabilities and the roton spectrum of a quasi-1D Bose-Einstein condensed gas with dipole-dipole interactions, Eur. Phys. J. D **31**, 439 (2004).

[49] S. Sinha and L. Santos, Cold dipolar gases in quasi-one-dimensional geometries, Phys. Rev. Lett. **99**, 140406 (2007).

[50] S. Pal, D. Baillie, and P. B. Blakie, Excitations and number fluctuations in an elongated dipolar Bose-Einstein condensate, Phys. Rev. A **102**, 043306 (2020).

[51] R. M. Wilson, C. Ticknor, J. L. Bohn, and E. Timmermans, Roton immiscibility in a two-component dipolar Bose gas, Phys. Rev. A **86**, 033606 (2012).

[52] A.-C. Lee, D. Baillie, P. B. Blakie, and R. N. Bisset, Miscibility and stability of dipolar bosonic mixtures, Phys. Rev. A **103**, 063301 (2021).

[53] W. Kirkby, T. Bland, F. Ferlaino, and R. N. Bisset, Spin rotons and supersolids in binary antidipolar condensates, SciPost Phys. Core **6**, 084 (2023).

[54] Progress has recently been made in creating stable spin mixtures of Dy atoms; see Refs. [41,45].

[55] H.-Y. Lu, H. Lu, J.-N. Zhang, R.-Z. Qiu, H. Pu, and S. Yi, Spatial density oscillations in trapped dipolar condensates, Phys. Rev. A **82**, 023622 (2010).

[56] S. Yi and H. Pu, Vortex structures in dipolar condensates, Phys. Rev. A **73**, 061602(R) (2006).

[57] R. M. Wilson, S. Ronen, J. L. Bohn, and H. Pu, Manifestations of the roton mode in dipolar Bose-Einstein condensates, Phys. Rev. Lett. **100**, 245302 (2008).

[58] S. Ronen, D. C. E. Bortolotti, and J. L. Bohn, Radial and angular rotons in trapped dipolar gases, Phys. Rev. Lett. **98**, 030406 (2007).

[59] T. Regge, Free boundary of He II and Feynman wave functions, J. Low Temp. Phys. **9**, 123 (1972).

[60] F. Dalfovo, Structure of vortices in helium at zero temperature, Phys. Rev. B **46**, 5482 (1992).

[61] W. E. Shirley, B. M. Anderson, C. W. Clark, and R. M. Wilson, Half-quantum vortex molecules in a binary dipolar Bose gas, Phys. Rev. Lett. **113**, 165301 (2014).

[62] W. Kirkby, A.-C. Lee, D. Baillie, T. Bland, F. Ferlaino, P. B. Blakie, and R. N. Bisset, Excitations of a binary dipolar supersolid, Phys. Rev. Lett. **133**, 103401 (2024).

[63] For discussions of the momentum-dependent effective interaction in single-component dipolar gases, see, e.g., Refs. [14,70,71].

[64] Note that while the dispersion relation is calculated for the homogeneous system, the numerical simulations introduce a small finite-size effect due to the presence of the soliton. As a result, the critical value of a_{12} is approximately 1% higher in Figs. 2(a2) and 2(b2) than in Figs. 2(a1) and 2(b1).

[65] C. Qu, L. P. Pitaevskii, and S. Stringari, Magnetic solitons in a binary Bose-Einstein condensate, Phys. Rev. Lett. **116**, 160402 (2016).

[66] T. Bland, E. Poli, L. A. P. Ardila, L. Santos, F. Ferlaino, and R. N. Bisset, Alternating-domain supersolids in binary dipolar condensates, Phys. Rev. A **106**, 053322 (2022).

[67] S. Li, U. N. Le, and H. Saito, Long-lifetime supersolid in a two-component dipolar Bose-Einstein condensate, Phys. Rev. A **105**, L061302 (2022).

[68] T. Bland, K. Pawłowski, M. J. Edmonds, K. Rzążewski, and N. G. Parker, Interaction-sensitive oscillations of dark solitons in trapped dipolar condensates, Phys. Rev. A **95**, 063622 (2017).

[69] In Fig. 3, the highest value of a_{12} considered is at least $1a_0$ below this threshold.

[70] P. B. Blakie, D. Baillie, and R. N. Bisset, Depletion and fluctuations of a trapped dipolar Bose-Einstein condensate in the roton regime, Phys. Rev. A **88**, 013638 (2013).

[71] R. N. Bisset, P. B. Blakie, and S. Stringari, Static-response theory and the roton-maxon spectrum of a flattened dipolar Bose-Einstein condensate, Phys. Rev. A **100**, 013620 (2019).

[72] C. Qu, M. Tylutki, S. Stringari, and L. P. Pitaevskii, Magnetic solitons in Rabi-coupled Bose-Einstein condensates, Phys. Rev. A **95**, 033614 (2017).